Revisiting doping mechanisms of n-type organic materials with N-DMBI for thermoelectric applications: Photo-activation, thermal activation, and air stability

Olivier Bardagot, Cyril Aumaître, Anthony Monmagnon, Jacques Pécaut, Pierre-Alain Bayle, Renaud Demadrille

Revisiting Doping Mechanisms of n-Type Organic Materials with N-DMBI for Thermoelectric Applications: Photo-Activation, Thermal Activation, and Air Stability.

Olivier Bardagot, Cyril Aumaître, Anthony Monmagnon, Jacques Pécaut, Pierre-Alain Bayle, Renaud Demadrille**

Affiliation: Université Grenoble Alpes/CEA/CNRS - IRIG-SyMMES - Grenoble 38000, France

Authors to whom correspondence should be addressed:

Dr. Olivier Bardagot, olivier.bardagot@dcb.unibe.ch

Dr. Renaud Demadrille, renaud.demadrille@cea.fr

Abstract

Understanding doping mechanisms is essential for optimizing the doping efficiency and rationally designing next generations of dopants and organic materials. Over the last years, N-DMBI became a reference solution-processed n-type dopant, affording decent air-stability and record power factor for thermoelectric energy generation. Nevertheless, a complete description of doping mechanism including the activation conditions, the doping pathways and possible side reactions is still lacking. In this work, we combined experimental and theoretical evidences to clarify the activation conditions of N-DMBI and elucidate the prevalent doping pathway depending on the dielectric constant of the medium. In polar media, direct doping *via* hydride H^- transfer is largely dominant while, in apolar media, SOMO-mediated doping after $H^{\bullet}$ release is thermodynamically favoured. We show that N-DMBI can be activated not only by thermal annealing above 100°C, but also by UV-light irradiation at low fluences even in thin films. Our findings stress the importance of working in strictly anoxic environment to avoid parasitic O_2-mediated side reactions, even in presence of a host.

Recently, remarkable progress of conducting polymers in terms of electrical properties opened up the field of thermoelectricity to organic semiconductors (OSCs).[1,2] For thermoelectric applications organic materials reveal some unique advantages such as low thermal conductivity, low cost, and ease of process on flexible substrates.[3,4] Since pioneer works dating from the last century,[5,6] molecular engineering and optimization of the doping process allowed to significantly improve the thermoelectric performances of doped OSCs reaching electrical conductivity (σ) beyond 2 x 10^5 S cm^{-1} (equivalent to platinum).[7] One of the most popular doping method of OSCs implies ion-pair formation *via* direct electron transfer.[8,9] This mechanism has been extensively studied for p-doped materials using various organic and inorganic dopants (halogens[10], strong Lewis acid[11] (*e.g.* $FeCl_3$[7]), or π-conjugated accepting molecules (*e.g.* F4TCNQ[12]), affording σ over 100 S cm^{-1} for many p-type polymers.[13] Comparatively, no n-doped OSC is reported with σ over 20 S cm^{-1} to date. One reason for the delayed development of highly conductive n-doped systems is their lower air-stability.[14] For p-doping *via* direct electron transfer, electrons are transferred from the OSC-HOMO to the dopant-LUMO, while for n-doping, electrons are transferred to the OSC-LUMO from the dopant-HOMO, therefore involving energy levels of much higher energies (lower ionization potentials).[9] If these levels are above the reduction potential of O_2/H_2O, n-doped systems are chemically unstable at air.

To tackle air-instability of n-dopants, the solution-processable small molecule (4 (1,3 dimethyl-2,3-dihydro-1H-benzoimidazol-2-yl)phenyl)dimethylamine (N-DMBI, named N-DMBI-H in this manuscript to emphasize the presence of the labile hydrogen atom) has been introduced as n-dopant precursor (Figure 1).[15] It was associated with various hosts such as carbon nanotubes[16], conductive polymers[17], and fullerene derivatives which led to the highest figure of merit ever reported for single-host organic thermoelectrics (ZT = 0.34 at 120°C).[18] We summarized some recent uses of N-DMBI-H in the organic thermoelectric field in Table S1.

N-DMBI-H doping mechanism is remarkable as, in most cases, it does not involve direct electron transfer but a two-step process comprising an activation step.[13] The doping pathways currently admitted are presented in Figure 1. The essential role of the –H atom was confirmed by the lost of the doping ability when substituting –H by a methyl group.[19]

In 2013, spontaneous doping of $PC_{61}BM$ *via* heterolysis bond cleavage (pathway I) was evidenced in solution (chlorobenzene) without heating.[20] The postulated mechanism involves a two-step process with (i) a bimolecular hydride transfer from N-DMBI-H to the fullerene, followed by (ii) an electron transfer from the hydride-reduced $PC_{61}BM\text{-}H^-$ to the unreduced $PC_{61}BM$ to form the $PC_{61}BM^{\bullet-}$ radical anion. Nonetheless, a hydrogen atom transfer was not completely ruled out in this study. Such mechanism remains an exception in the field and has never been evidenced with n-type polymers. In contrast, recent density functional theory (DFT)-supported mechanistic studies suggest that pathway II is the dominant mechanism when thermal annealing is performed on solid-state films.[21,22] Pathway II is characterized by an homolysis bond cleavage of the weak C-H bond, forming the neutral N-DMBI$^\bullet$ radical with a singly occupied molecular orbital (SOMO) level DFT-calculated at *ca.* -2.4 eV[19,23] .

In this work, we found a SOMO level lying at -2.70 eV based on bond dissociation energy (BDE) calculations starting from coordinates obtained by single-crystal X-Ray diffraction (XRD) (.cif files in SI). The doping effect then occurs by spontaneous electron transfer from the unstable radical-SOMO to the host-LUMO. Lastly, pathway III involves the direct electron transfer from the N-DMBI-H-HOMO (at -4.4 eV[23,24]) to the host-LUMO. Only few exceptions were reported[23,25] as such pathway is thermodynamically non favourable for most of host materials due to LUMO levels superior to -4.4 eV (Table S1). Note that, in all reports, the doping procedure involves a thermal activation step (Table S1). Previously reported examples of n-doping with N-DMBI-H in the solid state involve post-deposition thermal treatments (Table S1). This thermal step is claimed to activate the dopant, suggesting that the Gibbs free

energy is positive at RT (with $\Delta H > 0$ and $\Delta S > 0$).[19] Providing external energy seems therefore primordial to trigger activation of N-DMBI-H dopant precursor.

Insert Figure 1

Figure 1: Different n-doping pathways reported for N-DMBI-H dopant precursor. The neat molecule is named N-DMBI-H to emphasize the presence of the labile hydrogen atom, while the neutral imidazoline radical is written N-DMBI•. Italic: Energy levels (DFT).

Herein, we demonstrate a convenient way to activate N-DMBI-H using UV-light in solution at room temperature (RT). We bring experimental evidences for unravelling the photo-activation mechanisms of N-DMBI-H, and we highlight the influence of the dielectric constant of the media in the prevalence of pathway I and II. In this study, we also disclose degradation pathways and clearly show the crucial importance of working in anoxic environments with degassed solvents to avoid parasitic O_2-mediated side reactions.

The photo-activation of the dopant has been speculated but never demonstrated.[15,20] As a first approach, we monitored the evolution of absorbance spectra of N-DMBI-H solutions under diffuse daylight exposure and under dark conditions (Figure 2).

Insert Figure 2

Figure 2: Evolution of UV-Vis absorbance spectra of neat N-DMBI-H over time when kept in dark and exposed to ambient diffuse daylight in solution in chloroform (stabilized by ethanol).

Absorbance spectra show the conversion of N-DMBI-H into a species with a characteristic absorption band centred at ~350 nm. Dark control experiment revealed no obvious change after 105 minutes, confirming the role of light in the mechanism. The activation reaction under controlled UV-light of different intensities is shown in Figure S1. This experiment shows that

the kinetic of conversion depends on the irradiation power. The N-DMBI-H solutions were previously degassed to prevent O2-mediated side reactions. The isosbestic point at *circa* 315 nm (Figure 2) confirms a 1-to-1 chemical reaction without formation of side products.

In order to identify the product(s) obtained upon light irradiation, we solubilized N-DMBI-H in acetonitrile in acetonitrile (**polar** aprotic, ε = 37.5) and toluene (**apolar** aprotic, ε = 2.38), exposed the solutions to daylight, and crystallized the formed products by slow evaporation of the solvents at air. The structures were solved by single-crystal XRD. Crystal 2 was obtained from acetonitrile, crystal 3 from toluene. They are compared to neat N-DMBI-H (crystal 1) in Figure 3.

Insert Figure 3

Figure 3: Crystallographic data of neat N-DMBI-H (crystal 1) and photo-induced products obtained from acetonitrile (crystal 2) and from toluene (crystal 3) solutions. Simplified reaction pathways highlighting the impact of the dielectric constant of the medium. Θ is the dihedral angle between the average planes formed by the benzimidazole moiety (green plane) and the phenyl ring (red plane).

The analysis of crystal 1 confirms the presence of the hydrogen atom (H1) on the sp3 carbon (C1) which induces a strong torsion angle between the benzimidazole and the benzene dimethylamine plane (~97°, Table S2). Exposing N-DMBI-H in acetonitrile to daylight at air leads to N-DBMI$^+$ cation (crystal 2, Table S3). This conclusion is supported by: (i) the disappearance of the H1 hydrogen atom, (ii) the partial planarization of the molecule suggesting that C1 turned into a sp2 carbocation, (ii) the shorter C1-N1 and C1-N2 bond lengths characteristic of C-N double bonds (~1.34° Å *vs* 1.47 Å) (Figure S3). The structure of the counter-anion could not be solved (Table S2), however a similar structure stabilized by chloride ions (Cl^-) was found when reproducing the experiment in chloroform (crystal 2', Figure S3). In this case, chlorine ions are available from traces of HCl usually present in $CHCl_3$ because of its decomposition into toxic phosgene and HCl when exposed to molecular oxygen and UV-light. The presence of Cl^- increases the overall dielectric constant of pure chloroform (apolar, ε =

4.81) which can hence be compared to acetonitrile. The formation of N-DMBI$^+$ cation in $CDCl_3$ upon UV-light irradiation (λ=[315-435 nm]) was confirmed by the complete assignment of the NMR signals for this molecule (based on ^1H and ^{13}C NMR experiments, Figure S7, Figure S8 and Figure S9) and the comparison with the ones of N-DMBI-H. The disappearance of the NMR signal of H1 (4.8 ppm) and the absence of electron spin resonance (ESR) signal (Figure S4), confirmed the cationic nature of this specie. The carbocation is stabilized by donating mesomeric effect (+M) exerted by the two tertiary amines of the benzimidazole and the phenyl ring. In presence of a host, the stability of the doped system is therefore expected to be dominated by the stability of the reduced host (polymer or small molecule).

Interestingly, performing the same experiment in apolar solvents revealed a radically different behaviour. Exposing N-DMBI-H in toluene to daylight at air results in the formation of an amide derivative of N-DMBI (crystal 3, Table S4, Figure 3). The same result was obtained in chlorobenzene. Such DMBI-derived amide structure was already reported as side product obtained during the synthesis of DMBI-dimers.[26] We speculate a radical-induced $^3O_2$-mediated degradation pathway, which argues in favour of the preferential homolysis of the C-H bond in apolar media (pathway II). A mechanism explaining the formation of the DMBI-derived amide is proposed in Figure S6 (referred to as pathway IV). On the contrary, in polar media, N-DMBI$^+$ cation is favourably formed, likely through a hydride release stabilized by the polarity of the medium (pathway I).

To support our speculations and gain insights on the energetics of the competing I and II activation pathways, the Gibbs free energy changes of the following rate-limiting reactions were calculated by DFT:

$$\text{N-DMBI-H} \leftrightharpoons \text{N-DMBI}^+ + \text{H}^- \qquad \text{(heterolysis, cf. pathway I)}$$

$$\text{N-DMBI-H} \leftrightharpoons \text{N-DMBI}^\bullet + \text{H}^\bullet \qquad \text{(homolysis, cf. pathway II)}$$

The molecule geometries were optimized using the B3LYP-D3/TZ2P approach starting from the experimental set of Cartesian coordinates obtained by single-crystal XRD. The geometry of the neutral N-DMBI• radical was DFT-optimized starting from the cation structure. Solvation effects were investigated by performing the same calculations in different continuum polarizable models set for acetonitrile (polar) and toluene (apolar). The Gibbs free energy changes of the reactions of heterolysis and homolysis were calculated as follow: ΔG_{298} = G(products) - G(reactant), with G=H-TS, and reported in Table 1. The H and S values calculated for each reactants and products are reported in Table S5.

Solvent model	ΔG_{298} heterolysis	ΔG_{298} homolysis
Acetonitrile	+29.19 kcal/mol	+75.40 kcal/mol
Toluene	+78.92 kcal/mol	+74.97 kcal/mol

Table 1: Summary of Gibbs free energy changes to release a hydride anion (pathway I) or a hydrogen atom (pathway II) at T = 298.15K.

All ΔG_{298} are positive, confirming that these reactions are not spontaneous at RT neither in acetonitrile nor in toluene. In acetonitrile, the heterolysis is found thermodynamically more favourable than the homolysis, hence supporting our previous statement and in accordance with the enthalpy change reported.[27] By opposition, ΔG_{298} heterolysis and ΔG_{298} homolysis are similar in toluene, thereby suggesting a competition between these two reactions. Note that $\Delta G_{300} \approx 20.3$ kcal/mol (84.9 kJ/mol) was found experimentally in toluene in presence of fullerene.[20] In comparison to Table 1, this lower value underlines the decrease of the activation energy barrier due to host:N-DMBI-H dipolar interactions and the propensity of the host to form C-H bond, as suggested by Naab and coworkers.[20] However, our calculations strongly suggest that the dielectric constant of the medium has an influence on the prevalence of the activation mechanism of N-DMBI-H: pathway I being dominant in polar media, whereas pathway II is slightly favoured in apolar media.

We believe that these different mechanisms can take place when N-DMBI dopes organic semiconductors of different polarity in the solid state. This might explain why polar side chains facilitates molecular doping leading to increased doping efficiency and electrical conductivity.[28]

The thermal activation of N-DMBI is well established; however, the required temperature remains uncertain. Post-deposition thermal annealing ranging from 80°C to 150°C is generally applied, depending on the experimenter and the host material without a clear rationale (Table S1). In the literature, thermogravimetric analysis (TGA) has revealed that N-DMBI is a stable compound up to 200°C under inert atmosphere (N_2) before decomposition[21]. In another article, a slight gain of mass above 90°C was evidenced and assigned to oxidation.[18]

To shed light on the behaviour of N-DMBI upon thermal annealing, we heated up N-DMBI-H powder at 120°C for 2 hours in ambient conditions and analysed the residue without purification. The UV-Vis absorbance and NMR spectra of the residue are compared to the signatures of the neat N-DMBI-H, the N-DMBI$^+$ cation and the crystal 3 mainly composed of the amide derivative (Figure 4).

Insert Figure 4

Figure 4: (a) UV-Vis absorbance spectra and (b) corresponding ^{1}H NMR spectra in $CDCl_3$ of (from top to bottom): N-DMBI-H under dark conditions, after UV-light irradiation (λ=[315-435 nm], F1-30W/15 min, N-DMBI$^+$ cation), crystal 3 (from toluene), and the residue of N-DMBI-H heated at 120°C for 2 hours under ambient conditions.

The UV-Vis spectrum of the residue (blue line) reveals an absorption band centred at ~310 nm, similar to crystal 3 (Figure 4 a). The comparison with the NMR spectra indicates an almost complete conversion of N-DMBI-H into the amide derivative upon annealing at 120°C/2h at air (Figure 4 b). A total attribution is given in Figure S10. Performing TGA under O_2 gas flow allows to monitor the gain of mass induced by the oxidation (Figure S11). The onset of mass

gain is found at 100°C, reaching a maximum of +4.8% at 180°C. We can therefore conclude that: (i) the temperature to trigger N-DMBI activation is ~100°C, and (ii) the dominant mechanism is pathway II (cf. pathway IV). The C-H homolysis leads to the generation of unstable N-DMBI• radical that readily reacts with $^3O_2$ to form the amide derivative. In other words, the presence of molecular oxygen during N-DMBI-H activation leads to the formation of an amide degradation product that decreases the doping efficiency and acts as a morphological impurity, thus likely reducing the overall doped layer conductivity.

As a take-home message, N-DMBI-H activation must be triggered in a strictly anoxic environment to maximize the doping effect and the conductivity enhancement. It is interesting to note that crystal 3 is not only composed of the amide but also of N-DMBI$^+$ cation (absorption band at ~350 nm, NMR doublet of doublet at ~7.65 ppm, Figure S7). The presence of both species demonstrates the competition of hetero- and homolysis pathways in toluene, in accordance with the small difference of Gibbs free energy found by DFT (Table 1).

To illustrate the extreme sensitivity of N-DMBI-H to O_2 in a practical n-doping example, we blended N-DMBI-H with P(FBDOPV-2T-C_{12}), a polymer recently synthesized in our laboratory (Figure 5 a).[24] An electrical conductivity of 4.2 x 10^{-2} S cm^{-1} after thermal annealing can be achieved with this system. Doped films of P(FBDOPV-2T-C_{12}) exhibit thermoelectric properties, with a negative Seebeck coefficient of -265 μV K^{-1} and a thermoelectric power factor (PF) of 0.30 μW m^{-1} K^{-2} at 303 K that rises up to 0.72 μW m^{-1} K^{-2} at 388 K.

In an argon-filled glovebox, aliquots of a freshly prepared P(FBDOPV-2T-C_{12}):N-DMBI-H (62 mol%) anhydrous chlorobenzene solution stirred at RT (t0), 100°C (5, 10, 30, 60, 90 minutes) and allowed to cool down to RT (1080 minutes) were collected and analysed by ESR at RT (Figure 5 b).

Insert Figure 5

Figure 5: (a) Chemical structures of the n-type polymer (regiorandom x+y with x: R_1=$C_{12}H_{25}$, R_2=H; y: R_1=H, R_2= $C_{12}H_{25}$) and N-DMBI used to evidence O_2 consumption. (b) ESR spectra of doped-P(FBDOPV-2T-C_{12}), stirred at RT at t0 (black line), 100°C from 5 to 90 min, RT after (red line), in solution in anhydrous chlorobenzene (ESR tubes prepared in Ar-filled glovebox, O_2 < 10 ppm, dark conditions). Evolution of the signal (c) linewidth and (d) intensity (double integration) as a function of the stirring time at RT at t0, 100°C from 5 to 90 min, RT after.

The blend system exhibits an ESR signal at RT, indicating unpaired radicals. Interestingly, heating up the solution induced a decrease of the ESR signal linewidth (Figure 5 c). In biological studies, the correlation of the ESR signal linewidth with the O_2 content is common.[29,30] Heisenberg spin exchanges with paramagnetic O_2 cause a broadening of the linewidth.[31] We can therefore correlate the decrease of the signal linewidth with the consumption of O_2 in the solution over time. A sudden drop of the number of radicals is observed after 5 minutes at 100°C (Figure 5 d), suggesting a first step in which N-DMBI• is consumed through O_2-mediated reactions according to the mechanism proposed for pathway IV (Figure S6). In a second step, the progressive consumption of O_2 goes on (Figure 5 c) but an increase of radicals is observed (Figure 5 d). We can conclude that the effective doping of the polymer backbone is competing with side reactions involving O_2 reduction. Considering the low polarity of chlorobenzene (apolar, $\varepsilon = 5.69$), this finding is consistent with the prevalence of pathway II in apolar media. O_2-mediated reactions are detrimental for the overall doping efficiency and should be considered when hot processing is required for material deposition, or when pre-activation in solution is performed.

Thought this study of the single molecule dissociation of N-DMBI-H combining UV-Vis absorption, single-crystal XRD, DFT, NMR, TGA and ESR experiments, we clarified the necessary conditions to thermo- and photo-activate N-DMBI-H for n-doping. We determined that, in the solid state, a temperature superior to 100°C is required to trigger N-DMBI-H

activation *via* C-H homolysis bond cleavage. We evidenced the prompt oxidation of the resulting N-DMBI• radical, forming an inactive amide by-product. We highlight that molecular oxygen should be strictly avoided during N-DMBI-H doping process, even for hosts considered as air-stable in their doped state. Therefore, for a better control of the doping process, N-DMBI-H and N-DMBI-H:host blend solutions should be prepared in dark conditions using degassed solvents and post-deposition activation should also be performed in inert atmosphere. Finally, we show that the doping mechanism in solution (C-H heterolysis *versus* C-H homolysis) is influenced by the dielectric constant and the nature of the solvent used. In polar media (*e.g.* acetonitrile or e.g. acetonitrile or chloroform containing Cl^- from degradation): heterolysis bond cleavage is largely dominant, indicating direct doping *via* hydride H^- transfer. In apolar media (*e.g.* chlorobenzene or toluene): homolysis bond cleavage is dominant, indicating SOMO-mediated doping after H• release, however a non-negligible contribution of heterolysis should be considered. Alternatively to thermal activation, we demonstrate that photo-activation of N-DMBI-H is possible under UV-light irradiation, even at fluences as low as diffuse daylight. To illustrate the practical benefit of this finding, we show that P(FBDOPV 2T C12) thin films can be doped with N DMBI using UV-light irradiation only (Figure S12). This result opens up the way to high-resolution doping patterning using shadow masks. Our findings bring important guidelines for the development of N-DMBI-H doped systems applicable in thermoelectrics and organic electronics.

Supplementary Material

See supplementary material for UV-Vis absorption spectra, Single-crystals X-ray diffraction data, ESR and NMR spectra, DFT calculation, and thermogravimetric analysis of the compounds, detailed doping and degradation mechanisms, and photo-induced n-doping experimental data in thin films.

The data that supports the findings of this study are available within the article and its supplementary material.

The authors acknowledge the ANR for funding through the HARVESTERS project (ANR-16-CE05-0029-01) and the LABEX Laboratoire d'Alliances Nanosciences-Energies du Futur (LANEF, ANR-10-LABX-51-01). O.B acknowledge CEA for financial support through a PhD Grant.

References

[1] B. Russ, A. Glaudell, J.J. Urban, M.L. Chabinyc, and R.A. Segalman, Nature Reviews Materials **1**, 1 (2016).
[2] C. Gayner and K.K. Kar, Progress in Materials Science **83**, 330 (2016).
[3] Y. Wang, L. Yang, X.-L. Shi, X. Shi, L. Chen, M.S. Dargusch, J. Zou, and Z.-G. Chen, Advanced Materials **31**, 1807916 (2019).
[4] Y.-Y. Hsieh, Y. Zhang, L. Zhang, Y. Fang, S.N. Kanakaraaj, J.-H. Bahk, and V. Shanov, Nanoscale **11**, 6552 (2019).
[5] H. Shirakawa, E.J. Louis, A.G. MacDiarmid, C.K. Chiang, and A.J. Heeger, J. Chem. Soc., Chem. Commun. 578 (1977).
[6] Y. Nogami, H. Kaneko, T. Ishiguro, A. Takahashi, J. Tsukamoto, and N. Hosoito, Solid State Communications **76**, 583 (1990).
[7] V. Vijayakumar, Y. Zhong, V. Untilova, M. Bahri, L. Herrmann, L. Biniek, N. Leclerc, and M. Brinkmann, Advanced Energy Materials **9**, 1900266 (2019).
[8] A. Mityashin, Y. Olivier, T.V. Regemorter, C. Rolin, S. Verlaak, N.G. Martinelli, D. Beljonne, J. Cornil, J. Genoe, and P. Heremans, Advanced Materials **24**, 1535 (2012).
[9] I.E. Jacobs and A.J. Moulé, Advanced Materials **29**, 1703063 (2017).
[10] J. Tsukamoto, Advances in Physics **41**, 509 (2006).
[11] B. Yurash, D.X. Cao, V.V. Brus, D. Leifert, M. Wang, A. Dixon, M. Seifrid, A.E. Mansour, D. Lungwitz, T. Liu, P.J. Santiago, K.R. Graham, N. Koch, G.C. Bazan, and T.-Q. Nguyen, Nature Materials (2019).
[12] D. Kiefer, R. Kroon, A.I. Hofmann, H. Sun, X. Liu, A. Giovannitti, D. Stegerer, A. Cano, J. Hynynen, L. Yu, Y. Zhang, D. Nai, T.F. Harrelson, M. Sommer, A.J. Moulé, M. Kemerink, S.R. Marder, I. McCulloch, M. Fahlman, S. Fabiano, and C. Müller, Nature Materials **18**, 149 (2019).
[13] Y. Lu, J.-Y. Wang, and J. Pei, Chem. Mater. **31**, 6412 (2019).
[14] D.M. de Leeuw, M.M.J. Simenon, A.R. Brown, and R.E.F. Einerhand, Synthetic Metals **87**, 53 (1997).
[15] P. Wei, J.H. Oh, G. Dong, and Z. Bao, J. Am. Chem. Soc. **132**, 8852 (2010).
[16] Q. Hu, Z. Lu, Y. Wang, J. Wang, H. Wang, Z. Wu, G. Lu, H.-L. Zhang, and C. Yu, Journal of Materials Chemistry A **8**, 13095 (2020).
[17] K. Shi, F. Zhang, C.-A. Di, T.-W. Yan, Y. Zou, X. Zhou, D. Zhu, J.-Y. Wang, and J. Pei, Journal of the American Chemical Society **137**, 6979 (2015).

[18] J. Liu, B. van der Zee, R. Alessandri, S. Sami, J. Dong, M.I. Nugraha, A.J. Barker, S. Rousseva, L. Qiu, X. Qiu, N. Klasen, R.C. Chiechi, D. Baran, M. Caironi, T.D. Anthopoulos, G. Portale, R.W.A. Havenith, S.J. Marrink, J.C. Hummelen, and L.J.A. Koster, Nature Communications **11**, 5694 (2020).
[19] P. Wei, J.H. Oh, G. Dong, and Z. Bao, Journal of the American Chemical Society **132**, 8852 (2010).
[20] B.D. Naab, S. Guo, S. Olthof, E.G.B. Evans, P. Wei, G.L. Millhauser, A. Kahn, S. Barlow, S.R. Marder, and Z. Bao, J. Am. Chem. Soc. **135**, 15018 (2013).
[21] S. Riera-Galindo, A. Orbelli Biroli, A. Forni, Y. Puttisong, F. Tessore, M. Pizzotti, E. Pavlopoulou, E. Solano, S. Wang, G. Wang, T.-P. Ruoko, W.M. Chen, M. Kemerink, M. Berggren, G. di Carlo, and S. Fabiano, ACS Appl. Mater. Interfaces **11**, 37981 (2019).
[22] Y. Zeng, W. Zheng, Y. Guo, G. Han, and Y. Yi, J. Mater. Chem. A **8**, 8323 (2020).
[23] D. Huang, H. Yao, Y. Cui, Y. Zou, F. Zhang, C. Wang, H. Shen, W. Jin, J. Zhu, Y. Diao, W. Xu, C. Di, and D. Zhu, Journal of the American Chemical Society **139**, 13013 (2017).
[24] O. Bardagot, P. Kubik, T. Marszalek, P. Veyre, A.A. Medjahed, M. Sandroni, B. Grévin, S. Pouget, T. Nunes Domschke, A. Carella, S. Gambarelli, W. Pisula, and R. Demadrille, Adv. Funct. Mater. 2000449 (2020).
[25] Y. Lu, Z.-D. Yu, R.-Z. Zhang, Z.-F. Yao, H.-Y. You, L. Jiang, H.-I. Un, B.-W. Dong, M. Xiong, J.-Y. Wang, and J. Pei, Angewandte Chemie International Edition **58**, 11390 (2019).
[26] S. Zhang, B.D. Naab, E.V. Jucov, S. Parkin, E.G.B. Evans, G.L. Millhauser, T.V. Timofeeva, C. Risko, J.-L. Brédas, Z. Bao, S. Barlow, and S.R. Marder, Chemistry - A European Journal **21**, 10878 (2015).
[27] X.-Q. Zhu, M.-T. Zhang, A. Yu, C.-H. Wang, and J.-P. Cheng, J. Am. Chem. Soc. **130**, 2501 (2008).
[28] J. Liu, L. Qiu, R. Alessandri, X. Qiu, G. Portale, J. Dong, W. Talsma, G. Ye, A.A. Sengrian, P.C.T. Souza, M.A. Loi, R.C. Chiechi, S.J. Marrink, J.C. Hummelen, and L.J.A. Koster, Advanced Materials **30**, 1704630 (2018).
[29] P. Danhier and B. Gallez, Contrast Media & Molecular Imaging **10**, 266 (2015).
[30] H.M. Swartz, K.J. Liu, F. Goda, and T. Walczak, Magnetic Resonance in Medicine **31**, 229 (1994).
[31] M.P. Eastman, R.G. Kooser, M.R. Das, and J.H. Freed, The Journal of Chemical Physics **51**, 2690 (1969).

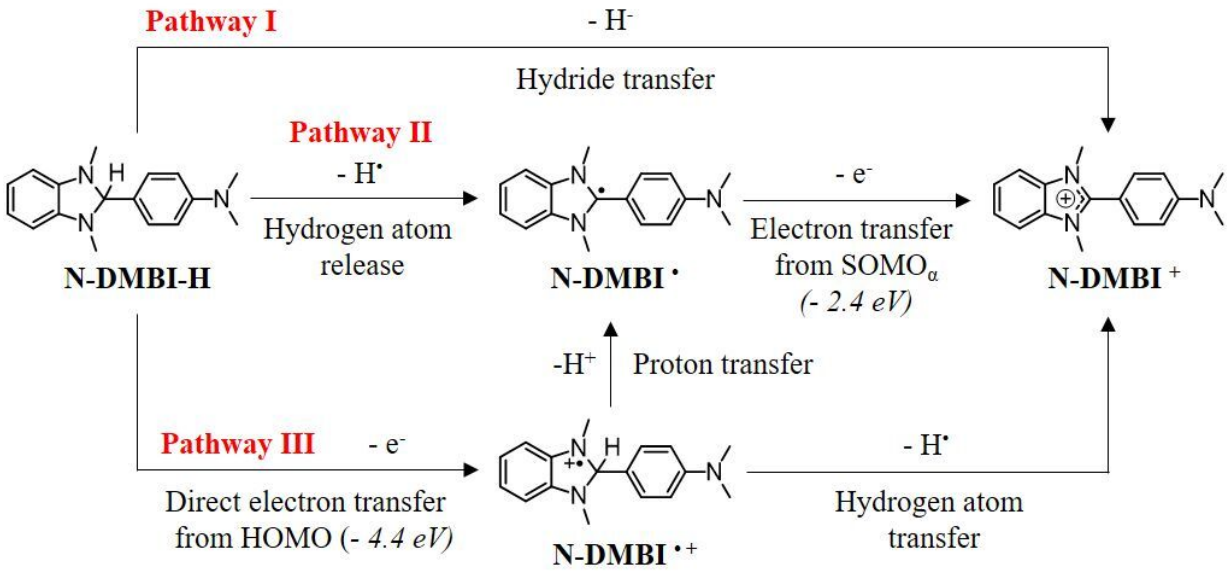

PLEASE CITE THIS ARTICLE AS DOI: 10.1063/5.0047637

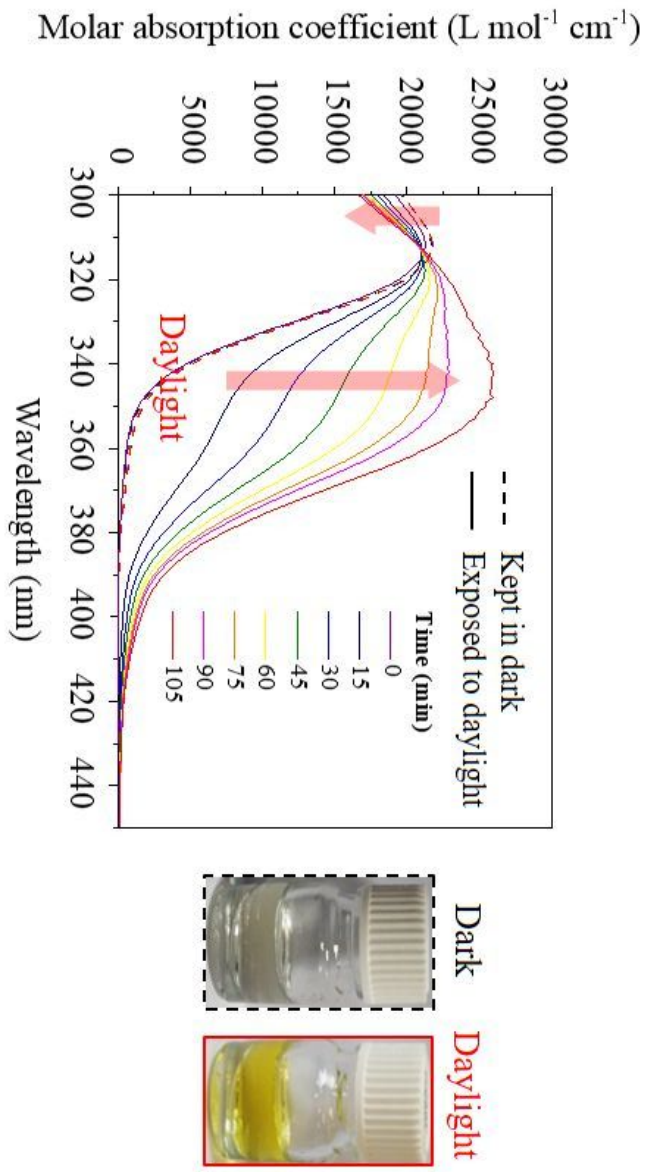

PLEASE CITE THIS ARTICLE AS DOI: 10.1063/5.0047637